

## Research article

Isabelle M. Palstra<sup>a</sup>, Hugo M. Doeleman<sup>a</sup> and A. Femius Koenderink<sup>\*</sup>

# Hybrid cavity-antenna systems for quantum optics outside the cryostat?

<https://doi.org/10.1515/nanoph-2019-0062>

Received February 27, 2019; revised April 19, 2019; accepted April 21, 2019

**Abstract:** Hybrid cavity-antenna systems have been proposed to combine the sub-wavelength light confinement of plasmonic antennas with microcavity quality factors  $Q$ . Here, we examine what confinement and  $Q$  can be reached in these hybrid systems, and we address their merits for various applications in classical and quantum optics. Specifically, we investigate their applicability for quantum-optical applications at noncryogenic temperatures. To this end we first derive design rules for hybrid resonances from a simple analytical model. These rules are benchmarked against full-wave simulations of hybrids composed of state-of-the-art nanobeam cavities and plasmonic-dimer gap antennas. We find that hybrids can outperform the plasmonic and cavity constituents in terms of Purcell factor, and additionally offer freedom to reach any  $Q$  at a similar Purcell factor. We discuss how these metrics are highly advantageous for a high Purcell factor, yet weak-coupling applications, such as bright sources of indistinguishable single photons. The challenges for room-temperature strong coupling, however, are far more daunting: the extremely high dephasing of emitters implies that little benefit can be achieved from trading confinement against a higher  $Q$ , as done in hybrids. An attractive alternative could be strong coupling at liquid nitrogen temperature, where emitter

dephasing is lower and this trade-off can alleviate the stringent fabrication demands required for antenna strong coupling. For few-emitter strong-coupling, high-speed and low-power coherent or incoherent light sources, particle sensing and vibrational spectroscopy, hybrids provide the unique benefit of very high local optical density of states, tight plasmonic confinement, yet microcavity  $Q$ .

**Keywords:** nanophotonics; plasmonics; microcavities; quantum optics; strong coupling.

## 1 Introduction

Microcavities are a key building block for all branches of optics, and over the last 30 years, their development has been a mainstay of micro- and nanoscale optics research efforts. For instance, vertical-cavity surface-emitting lasers in active III–V semiconductor systems are a key technology for optical interconnects in information processing in any data center. At the same time, the narrow spectral lines of microcavities are key for label-free sensing down to the level of single proteins [1], and for metrology of distances down to the picometer scale [2]. In quantum optics, microcavities are particularly sought after for their ability to turn intrinsically slow and isotropic emitters into directional and fast single-photon guns [3–5] and even to bring quantum emitters into strong coupling regimes where spontaneous emission is replaced by quantum entanglement of light and matter [6]. Notwithstanding the large diversity of microcavity designs, generally they are characterized by two figures of merit: the first relates to *temporal* and the second to *spatial* confinement. The quality factor  $Q$  measures the time duration for which light is stored in the resonator in units of optical cycles, while the mode volume  $V$  is a measure for how tightly light is confined in three dimensions. For actual applications, generally algebraic combinations of  $Q$  and  $V$  determine performance. For instance, the most well-known figure of merit for a cavity is undoubtedly the Purcell factor for

<sup>a</sup>Isabelle M. Palstra and Hugo M. Doeleman: These authors contributed equally to this work.

**\*Corresponding author: A. Femius Koenderink**, Center for Nanophotonics, AMOLF, Science Park 104, 1098 XG Amsterdam, The Netherlands; and Van der Waals-Zeeman Institute, Institute of Physics, University of Amsterdam, Science Park 904, PO Box 94485, 1090 GL Amsterdam, The Netherlands, e-mail: f.koenderink@amolf.nl. <https://orcid.org/0000-0003-1617-5748>

Isabelle M. Palstra and Hugo M. Doeleman: Center for Nanophotonics, AMOLF, Science Park 104, 1098 XG Amsterdam, The Netherlands; and Van der Waals-Zeeman Institute, Institute of Physics, University of Amsterdam, Science Park 904, PO Box 94485, 1090 GL Amsterdam, The Netherlands

spontaneous emission enhancement in a cavity, which reads [7]

$$F_p = \frac{3}{4\pi^2} \frac{Q}{\tilde{V}}, \quad (1)$$

where  $\tilde{V} = V/(\lambda/n)^3$  is the mode volume expressed in units of wavelength cubed in the medium of interest. This factor quantifies the local optical density of states (LDOS) at resonance [8, 9], and is thereby fundamental for many light-matter interactions, such as creating desirable single-photon sources [3] or building sensors for analytes that have optimum sensitivity [1, 10]. However, for other applications, ranging from spectral filters to optical memories, building lasers [11], enhancing nonlinear optical effects [12], and cavity quantum electrodynamics (QED) [6, 13], other metrics apply. For instance, in cavity QED the so-called regime of strong coupling is sensitive to  $Q/\sqrt{\tilde{V}}$  [6].

Approximately 15 year ago, plasmonics was proposed as the solution for the main perceived drawback of classical dielectric microcavities: whether in the form of microdisks, micropillars, or photonic crystals, dielectric cavities are limited in achievable confinement to approximately the diffraction limit, meaning that target performances tend to require minimum quality factors (typically  $Q > 10^4$ ). In contrast, plasmonic resonators have stellar confinement, but *exceptionally* poor  $Q$  in the order of 10. Indeed, plasmon nanoantenna resonators have been reported that provide measured Purcell factors up to  $10^3$  [14–16], and recent claims are that plasmon antennas allow quantum strong coupling with single emitters at room temperature, as opposed to at cryogenic temperatures as achieved in microcavities [17, 18]. Figure 1 shows quality factors and mode volumes of dielectric microcavities and plasmonic antennas that are at the state of the art. The striking observation is that even if similar Purcell factors are possible (constant  $F$  indicated by diagonals in the diagram), there is a huge gap between nanoantennas and microcavities.

Apparently, reaching *intermediate* ( $Q-\tilde{V}$ )-values, where one trades in part of the plasmonic confinement in favor of higher  $Q$ , is extremely difficult. This is unfortunate, as plasmonic quality factors ( $Q=10$ ), and the fact that they cannot be controlled at will, can hardly be classified as a practical proposition for many envisioned applications. Moreover, the extremely low antenna mode volumes require exceptional control over the spatial alignment of the emitter and antenna. On the other hand, the extremely narrow linewidths of high- $Q$  cavities make it difficult to couple to luminescent materials, which generally have much broader linewidths unless one works at cryogenic temperatures. Working in the cryostat, however, is not an ideal solution to these problems. In addition

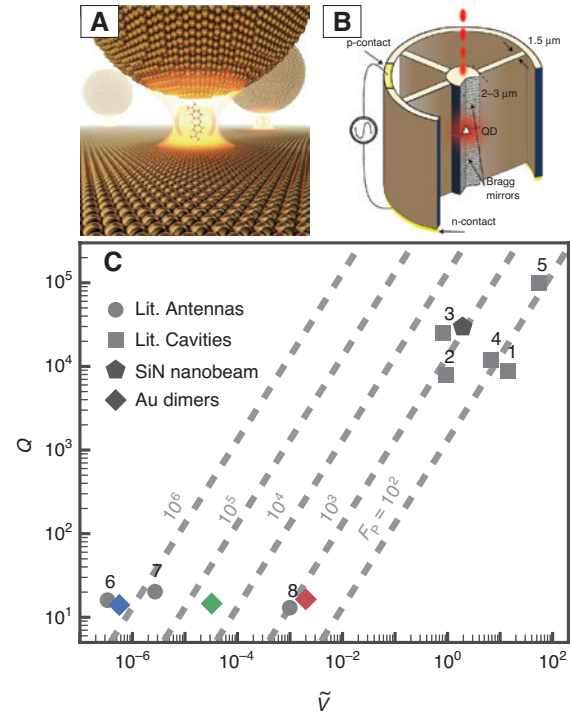


**Figure 1:** Reported quality factors and mode volumes for dielectric cavity and plasmonic antenna systems. (A, B) Renderings of state-of-the-art plasmonic [17] (A) and dielectric [19] (B) microcavities. (C)  $Q$  and  $\tilde{V}$  values for state-of-the-art cavities (1: [20], 2: [21], 3: [22], 4: [23], 5: [24]) and antennas (6: [17], 7: [18], 8: [15]). Also shown are values for the cavity and antennas used in this work – a silicon nitride (SiN) nanobeam cavity and gold dimer antennas with dimer gaps of 1 (blue), 5 (green) and 25 nm (red). Dashed lines indicate lines of the constant Purcell factor  $F_p$ . Image credits: Panel (A): reprinted with permission from Springer Nature, Nature, 2016;535:127–30, Copyright 2016. Panel (B): reprinted with permission from Springer Nature, Nature Photonics, 2016;10:340–5, Copyright 2016.

to high cost and reduced collection efficiency, matching narrow linewidths of different emitters and devices becomes highly challenging at high  $Q$ .

Recently, several groups including our own suggested that hybrid plasmonic-dielectric resonators can be constructed [25–41], raising the idea that exactly this trade-off between confinement and  $Q$  can be reached. In this work we present a survey of the performance that should be available with hybrids if one assumes access to state-of-the-art building block cavities and antennas. To this end we discuss full-wave calculations on actually envisioned combinations of constituents, and on the basis of a simple model, propose and benchmark a set of crucial design rules of thumb. Having mapped out that one can in principle indeed construct hybrids of even better  $Q/\tilde{V}$  than the constituents, yet at essentially any intermediate  $\tilde{V}$ , we critically examine if this is of any actual use toward several

applications, such as strong coupling with promising quantum emitters, bright single-photon sources, as well as high-speed light-emitting diodes (LEDs), low-threshold lasers, sensing and vibrational spectroscopy. We have to conclude that room-temperature strong coupling will be as difficult to achieve with hybrids as it is with plasmon antennas alone, although once you achieve it, you have full freedom of choice over linewidth. At the same time, we conclude that hybrids are unique for their very high Purcell factors at any  $Q$ , even if their confinement is not as good as that in the very best plasmon antenna. This characteristic may offer a pathway to single-emitter strong coupling at liquid nitrogen temperatures with many different types of emitters, and to bright, low-jitter single-photon sources that might reach indistinguishability yet even operate at room temperature. If these findings would be turned into actual reality in the laboratory, this could be of large practical importance given that one could finally pass the first litmus test of “practicability” that many of the now available, highly impressive solid-state quantum light-sources fail, namely that no liquid helium temperature is required.

## 2 A model system of dimer antennas coupled to a nanobeam cavity

To assess the potential of hybrid plasmonic-dielectric resonators we first numerically explore a model system using full-wave finite-element simulations. The model system is designed to overcome main limitations of our previous work [35], which was strictly confined to gapless single-particle antennas that intrinsically had quite poor LDOS enhancement characteristics, and which focused on cavities of intrinsically large mode volume. Here instead we obtain  $Q$ ,  $\tilde{V}$ , and the LDOS of dielectric-plasmonic hybrids consisting of a silicon nitride ( $\text{Si}_3\text{N}_4$ ) nanobeam cavity and a family of gold dimer antennas. The nanobeam cavity is among the smallest mode volume high- $Q$  cavities achievable in the near-infrared, while the gold dimer antennas offer LDOS enhancements in their gap that goes well beyond the enhancements possible with single-particle nanoantennas.

In the following sections, we first describe the separate components, followed by a discussion of the merits of the hybrid system.

### 2.1 The bare cavity and antenna

For the cavity, we focus on a  $\text{Si}_3\text{N}_4$  photonic crystal nanobeam with a design inspired by Deotare et al. [42]. As we

will show in Section 3, hybrid designs have best performance if the constituent cavity and antenna themselves offer high  $Q$  and low mode volume  $\tilde{V}$ . Photonic crystal nanobeam cavities have shown to be near-ideal cavity systems, with high confinements and quality factors [42–44], where  $\text{Si}_3\text{N}_4$  is a commonly used material for dielectric cavities designed to operate in the visible to near-infrared due to its low material losses and moderately high refractive index ( $n \approx 2$ ). Our nanobeam cavity consists of a rectangular beam that is 400 nm wide and 250 nm thick. Two sets of six cylindrical holes with a pitch of 300 nm and hole radii of 100 nm form photonic-crystal mirrors. Between these, a cavity is formed by a taper consisting of five holes, in which pitch and hole size are reduced linearly to 260 and 77 nm respectively toward the center of the cavity. The spacing between the edges of the two central holes is 52 nm. The central part of the cavity design is shown in Figure 2A and B.

Using the eigenmode solver of COMSOL Multiphysics, we calculate the eigenfrequency,  $Q$ , and field distribution of the fundamental mode, which is confined in the center of the beam (Figure 2A). We calculate the effective mode volume  $\tilde{V}_c$  for the cavity as follows:

$$\tilde{V}_c = \frac{\int \varepsilon(\vec{r}) |\vec{E}(\vec{r})|^2 d^3\vec{r} \left( \frac{n(\vec{r}_e)}{\lambda_{\text{vac}}} \right)^3}{\varepsilon(\vec{r}_e) |\vec{E}(\vec{r}_e)|^2}, \quad (2)$$

where  $\varepsilon$  is the dielectric constant,  $n$  is the refractive index,  $\vec{E}$  is the electric field amplitude,  $\lambda_{\text{vac}}$  is the wavelength in vacuum, and  $\vec{r}_e$  is the location of the emitter. This is the textbook definition for mode volume (ignoring the problems with it pointed out and resolved respectively in [45] and [46]), barring the fact that we evaluate the mode volume felt by an emitter centered at 25 nm *above the surface* of the beam, at position  $\vec{r}_e$ . This is significantly larger than the traditional mode volume that is referenced to the mode maximum, but appropriate for our envisioned antenna and emitter placement, since placing an antenna in the center of such a nanobeam cavity is not feasible. We find  $\tilde{V}_c \approx 2$ , within an order of magnitude of the diffraction limit ( $\tilde{V} = 1/2^3$ ). These values are similar to experimental and theoretical values reported previously in the literature [42–44], as shown by the hexagon in Figure 1. Though methods based on further slots taken out of the cavity have been proposed to reduce the mode volume even well below the diffraction limit [47–49], we will show that this does not significantly improve the performance of hybrids, which is why we choose the simpler cavity design. As verification of our eigenmode calculations, we have also performed driven dipole calculations to determine the LDOS spectrum, as shown in Figure 2C

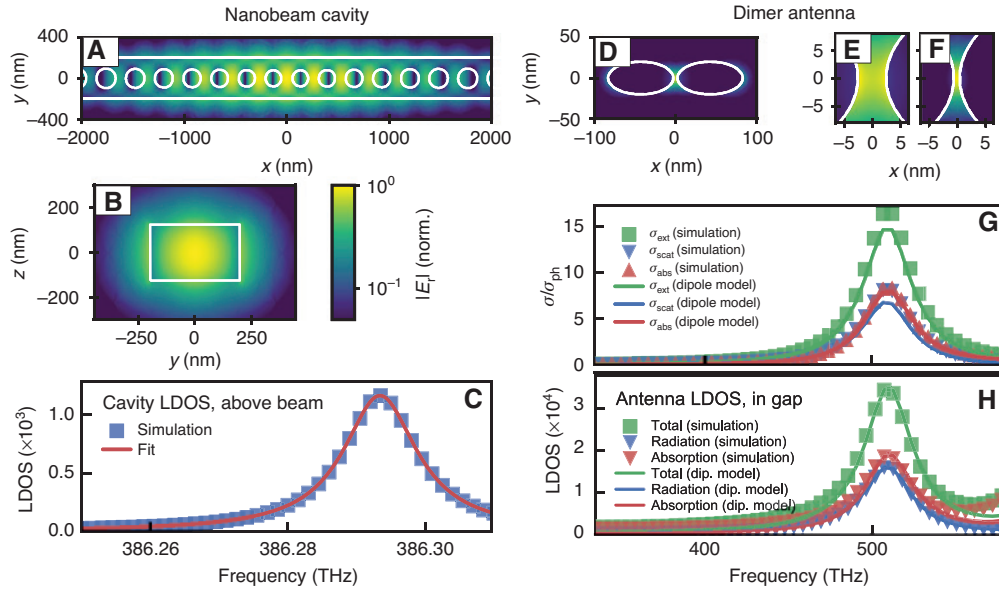


**Figure 2:** Properties of the separate components of the nanobeam cavity and the dimer antenna.

(A)  $x, y$  crosscut of the cavity design and of the field distribution in the cavity. We see that the field is confined in the central defect of the photonic crystal. (B)  $y, z$  crosscut in the center of the nanobeam cavity, showing that most of the field is centered in the high-index  $\text{Si}_3\text{N}_4$ . (C) The LDOS of the cavity system at 25 nm above the beam. It has a maximum value of  $1.16 \times 10^3$  and a width of 0.013 THz, which gives a  $Q$  of  $3.0 \times 10^4$ . (D) A crosscut of the plasmonic antenna. Clearly, most of the field is concentrated in the 5 nm gap between the metal particles. (E, F) Magnified images of the field profiles of the antennas with a gap separation of 5 and 1 nm, respectively. Note that all field profiles in (A, B) and (D–F) are normalized to their maxima and shown on a logarithmic scale. (G) Extinction, scattering and absorption cross-sections  $\sigma_{\text{ext}}$ ,  $\sigma_{\text{scat}}$  and  $\sigma_{\text{abs}}$ , respectively, of an antenna with  $L = 80$  nm and a gap of 5 nm, showing the increase of cross-sections at resonance. Cross-sections are normalized to the physical cross-section  $\sigma_{\text{ph}}$ . We compare values obtained directly from simulations and indirectly via a dipole model, showing good agreement. (H) The LDOS in the center of the antenna gap (same antenna as in (G)). It shows a peak at the dipolar resonance. Again, we find good agreement between our dipole model and the numerical simulations. Deviation at the highest frequencies is due to the onset of a multipolar resonance.

for a dipole above the central defect of the beam, 25 nm from the  $\text{Si}_3\text{N}_4$ . We find a maximum LDOS of  $1.16 \times 10^3$  at 386 THz and a linewidth of 0.013 THz, which corresponds to  $Q = 3.0 \times 10^4$  and  $\tilde{V}_c = 1.9$ . Throughout this work, quoted LDOS values are normalized to the LDOS in vacuum at the same frequency, and LDOS is understood to mean the sum of radiative and nonradiative effects (as contained in the imaginary part of the dyadic Green function [8]).

Next we turn to our model antenna system, for which we use a family of gold dimer ellipsoid antennas. Currently, the smallest mode volumes in plasmonics, reported to be as low as  $\lambda^3/10^6$  [17, 50], are achieved not in dimer gap antennas but in metal-insulator-metal (MIM) structures composed of nanoparticles on smooth metal films, separated by a dielectric spacer [51–55]. However, due to the peculiar metal-film geometry and the dominant out-of-plane polarization characteristics, these MIM antennas appear less amenable to hybrid integration with a cavity than, for example, nanorod and bow-tie antennas. In this work we choose dimer ellipsoid antennas for simplicity, ease of tunability, and high LDOS in the gap.

Their performance is similar to bow-tie antennas at equal gap sizes (see Supplementary material). We study dimers with widths of 40 nm, lengths  $L$  of 60, 80 and 100 nm (for a single ellipsoid), and gaps varying between 1 and 25 nm. The length controls the antenna resonance frequency and the antenna scattering strength. At the same time, tuning the gap tunes the LDOS enhancement at the antenna center. Figure 2D shows a crosscut of the field for one example case, with  $L = 80$  nm and a gap of 5 nm. As expected, most of the field is concentrated in the gap between the antennas (magnified image in Figure 2E). This confinement increases with decreasing gap size, as shown in Figure 2F for a gap of 1 nm.

As with the nanobeam, we perform finite element simulations on the antenna, now driving it with an incident plane wave polarized along its long axis. We can directly retrieve antenna scattering, extinction, and absorption cross-sections  $\sigma_{\text{scat}}$ ,  $\sigma_{\text{ext}}$ ,  $\sigma_{\text{abs}}$ , respectively, as shown by the data points in Figure 2G. We observe a resonance corresponding to an electric dipole mode, with an albedo (defined as  $A = \sigma_{\text{scat}}/\sigma_{\text{ext}}$ ) of roughly 50%. A comparison to

a dipole model, shown by the lines in Figure 2G and H, is discussed in Section 3. A simulation with a point source at the center of the antenna gap reveals a significant LDOS, peaking at  $3.4 \times 10^4$  at an apparent quality factor of  $Q=14$ , as shown in Figure 2H. Increasing antenna length  $L$  causes a redshift of this dipole mode and a slight increase of albedo (due to increased volume). As expected, decreasing the gap enhances both radiative and absorptive LDOS in a roughly equal manner. From these simulations we can retrieve the antenna quality factor  $Q_a$  and mode volume  $\tilde{V}_a$ , which are shown by the colored markers in Figure 1 for gaps of 1, 5 and 25 nm. Note that we use the term “mode volume” here *not* as an endorsement of the validity of this concept *per se* for plasmonics [45], and the term *neither* indicates that we employed a formula similar to Eq. (2) *nor* that we deployed a quasi-normal mode formalism [36, 46, 56]. Instead, we obtain antenna mode volume by *inversion* of Eq. (1), and use it as a metric for how high the LDOS enhancement is on resonance, given the antenna quality factor  $Q_a$ .

## 2.2 The hybrid systems

To determine the properties of hybrid systems, we perform simulations of our nanobeam cavity with a gold ellipsoid dimer placed on top of the beam (see Figure 3A). The dimer is placed above the center of the beam (antenna gap center is 25 nm above the surface of the beam). The long axis is aligned in the  $y$ -direction, matching the cavity mode polarization. Ellipsoid length is varied from 60 to 100 nm, and gap size from 1 to 30 nm. The source is placed at the center of the antenna gap, matching the source positions of both the bare antenna and cavity simulations. As an implementation note, in COMSOL we ensured that all calculations (for bare constituents and hybrid, driven, and eigenmode calculations) use the very same mesh, where we cycle through the distinct structures by setting material constants appropriately. This approach safeguards against small shifts in frequency and  $Q$  that can occur as a function of mesh and geometry truncation in COMSOL. Figure 3B and C show field profiles of the hybrid mode, obtained from eigenmode calculations (without source) for antennas with 40 and 80 nm short and long axes, and a 5-nm gap. In stark contrast with the bare cavity mode shown in Figure 2A and B, the hybrid mode is strongly concentrated around the antenna. Nonetheless, the mode  $Q$  remains high (order  $10^3$ ) and the waveguide crosscut also clearly shows energy density inside the beam. These characteristics indicate hybridization of the cavity and antenna. Figure 3D shows the LDOS spectra of

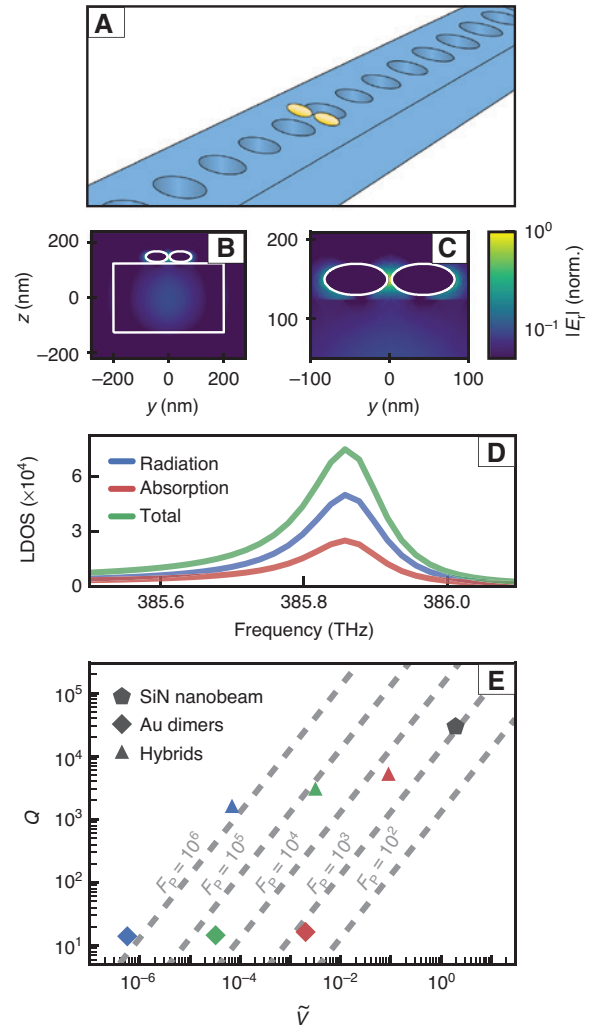


**Figure 3:** Properties of the hybrid system calculated with numerical simulations.

(A) Sketch of the hybrid system, with a gold dimer placed just above the center of a nanobeam cavity. (B) Crosscuts of the field profiles of the hybrid at  $x=0$ , with a gap of 5 nm. Contrary to the bare cavity shown in Figure 2B, here the field is strongly localized at the antenna. (C) Magnified image of (B), showing that locally the field resembles the bare antenna mode profile in Figure 2D. Fields in (B, C) are normalized to their maxima and shown on a logarithmic scale. (D) Numerically calculated radiative, absorptive and total LDOS of the hybrid. LDOS shows Fano lineshapes and we find a maximum total LDOS of  $7.5 \times 10^4$  at a  $Q$  of 3000, yielding  $\tilde{V}_H = 3 \times 10^{-3}$ . (E) Comparing a selection of hybrid systems with the bare cavity and antennas for different gap sizes. Dashed lines indicate lines of the constant Purcell factor  $F_p$ . Here we show gaps of 25 (red), 5 (green), and 1 nm (blue). Hybrid  $Q$  and  $\tilde{V}$  lie in between those of their constituents, and a decrease in  $\tilde{V}_a$  leads to a similar decrease in hybrid  $\tilde{V}$ .

a hybrid system with an antenna length of 80 nm and a gap size of 5 nm. We observe an LDOS peak of  $7.5 \times 10^4$  – a remarkable 64-fold (2.2-fold) increase over the bare cavity (antenna at resonance). Moreover, the lineshape

is no longer Lorentzian but slightly asymmetric; such a Fano lineshape is characteristic of interference between a narrow resonance and a broad background [57], and has been predicted by several groups to occur in the hybrid cavity-antenna system LDOS [27, 29, 35, 36, 41]. Strong enhancements of the LDOS, as compared to the bare components, have also been reported in theoretical studies of other hybrid systems [35, 36, 41]. LDOS can be further increased in our antenna-cavity systems using several tuning mechanisms (see the next section).

We now compare this hybrid system in terms of the resultant  $Q$  and  $\tilde{V}$  with the bare cavity and antenna. Hybrid and antenna  $Q$  are obtained through a fit with a Fano or Lorentzian lineshape, respectively. Mode volumes  $\tilde{V}$  are again obtained through the peak LDOS and inversion of Eq. (1). A selection of the obtained values for  $Q$  and  $\tilde{V}$  for our cavity, bare antennas and hybrids are shown in the phase diagram in Figure 3E. Clearly, the hybrids appear right in the intermediate regime, with  $Q$  and  $\tilde{V}$  between those of the cavity and antenna. Moreover, we see that hybrid systems always have higher LDOS than their individual constituents. This highlights the great potential of hybrids for practical devices that operate at intermediate  $Q$ , while maintaining high LDOS. We note that a large host of simulations of different antenna geometries (systematically varying dimer width, length, and gap size) and materials (silver and gold) all show similar behavior: hybrids show enhanced LDOS as compared to the cavity and antenna, Fano lineshapes, and a quality factor in between that of the cavity and antenna.

A salient feature of the data in Figure 3E is the proportional scaling of the hybrid mode volume with the antenna mode volume. As antenna mode volumes are reduced by narrowing the gap, the hybrid mode volume reduces equally. This raises the question: What determines hybrid  $Q$  and  $\tilde{V}$ , and what possibilities do we have to optimize these parameters? In the following section, we employ an analytical model to better understand the effects of the cavity and antenna on the properties of the resulting hybrids.

### 3 Hybrid system design rules

Different applications of resonators in classical and quantum optics will place different requirements on resonator frequency,  $Q$  and  $\tilde{V}$ . To design hybrids that meet such requirements, it is important to understand how the hybrid's properties depend on those of its constituents. Here we study these properties using an analytical

coupled oscillator model [35]. This model is generally valid for any cavity or antenna geometry, provided that:

1. the antenna can be treated as a dipolar scatterer, with no higher order multipole contributions in scattering, and
2. far-field radiation overlap between the cavity and antenna can be neglected, meaning that *interference* between far-field loss of the antenna and cavity can be neglected (if this is not the case, we refer to [58] for the unconventional resulting physics).

Furthermore, we assume that the near-field gap effects that imbue the antenna with a large local enhancement of LDOS as compared to a simple dipole picture can be lumped into a prefactor that does not change with environment (see Supplementary material). Although we expect that our systems fulfill both conditions, the purpose of this section is not to propose a perfect model, but instead to provide simple “rules of thumb” for hybrid system design. The strength of the coupled oscillator model is that it can predict the properties of a hybrid system, given those of the individual constituents. We fit the simulated cavity LDOS to retrieve cavity resonance frequency  $\omega_c$ , quality factor  $Q_c$ , and mode volume  $V_c$ , as shown in Figure 2C. From the antenna simulations we directly obtain antenna polarizability  $\alpha(\omega)$  (along the antenna long axis) by integrating the polarization currents in the antenna under plane wave driving. For a dipolar particle in a homogeneous medium, the polarizability  $\alpha$  should relate directly to  $\sigma_{\text{scat}}$  and  $\sigma_{\text{ext}}$  [59], so we can compare “dipolar” cross-sections (from retrieved polarizability) to the directly obtained cross-sections. Figure 2G shows good agreement, indicating that our antennas are indeed dominated by electric dipole resonances. The LDOS in a hybrid system is given by the coupled oscillator model as follows [35]:

$$\text{LDOS}_H = 1 + \frac{6\pi\epsilon_0 c^3}{\omega^3 n} \text{Im}\{\alpha_H G_{\text{bg}}^2 + 2G_{\text{bg}}\alpha_H\chi_c + \chi_H\}. \quad (3)$$

Here,  $n$  is the index of the background medium and  $\alpha_H = \alpha(1 - \alpha\chi_c)^{-1}$  is the hybridized antenna polarizability, that is, taking into account the cavity-antenna coupling. The response function  $\chi_c$  of the unperturbed cavity assumes a Lorentzian lineshape that is fully determined by  $\omega_c$ ,  $Q_c$ , and  $V_c$ , while that of the perturbed cavity is given as  $\chi_H = \chi_c(1 - \alpha\chi_c)^{-1}$ . The parameter  $G_{\text{bg}}$  represents the field scattered from the source to antenna and vice versa (i.e. Green's function of the background medium) and encodes for the antenna-source coupling. A decrease in antenna  $\tilde{V}$  is captured mainly by an increase in  $G_{\text{bg}}$ . It is obtained directly from the simulated (radiative) LDOS of the bare antenna, for which a similar expression as Eq. (3) can be

derived that depends on  $\alpha$  and  $G_{\text{bg}}$ . To verify the fidelity of this retrieval, we compare analytical expressions for LDOS to simulation data (Figure 2H), which show good agreement. For further details on the model and the retrieval of cavity and antenna parameters, we refer to the Supplementary material. The interpretation of Eq. (3) is, crudely speaking, that the LDOS in the hybrid is that of vacuum, plus three contributions. The first ( $\propto \text{Im}\{\alpha_{\text{H}} G_{\text{bg}}^2\}$ ) is the contribution of just an emitter coupled to a polarizable antenna, but with the caveat that the antenna polarizability is modified by the cavity. Conversely, the last term is exactly the LDOS one would expect from an emitter coupled to just a cavity, but with the caveat that the cavity is perturbed by the antenna. Thus  $\chi_{\text{H}}$  accounts for the change in frequency and  $Q$  predicted by cavity perturbation theory [60, 61]. Finally, the middle term contains interferences between antenna and cavity contributions.

We now study the influence of four parameters on the hybrid system properties – the antenna-cavity detuning, antenna mode volume  $V_{\text{a}}$ , and cavity  $Q$  and  $V_{\text{c}}$ . This leads to four design rules for a hybrid system, which we discuss below.

- **Rule of thumb I:** decreasing antenna-cavity detuning decreases hybrid  $Q$  and  $\tilde{V}$ , at roughly equal LDOS. Figure 4A shows hybrid LDOS spectra for four hybrids, each with different cavity frequency  $\omega_{\text{c}}$ . Each spectrum shows a broad peak at the bare antenna resonance and a narrow peak close to the bare cavity resonance. The width of this hybrid resonance, however, varies greatly with detuning. Figure 4B shows this dependence of  $Q_{\text{H}}$  (the hybrid  $Q$ ) on detuning more explicitly. Far red-detuned from antenna resonance,  $Q_{\text{H}}$  approaches the bare cavity  $Q$ , yet near resonance we see a decrease in  $Q_{\text{H}}$  of more than two orders

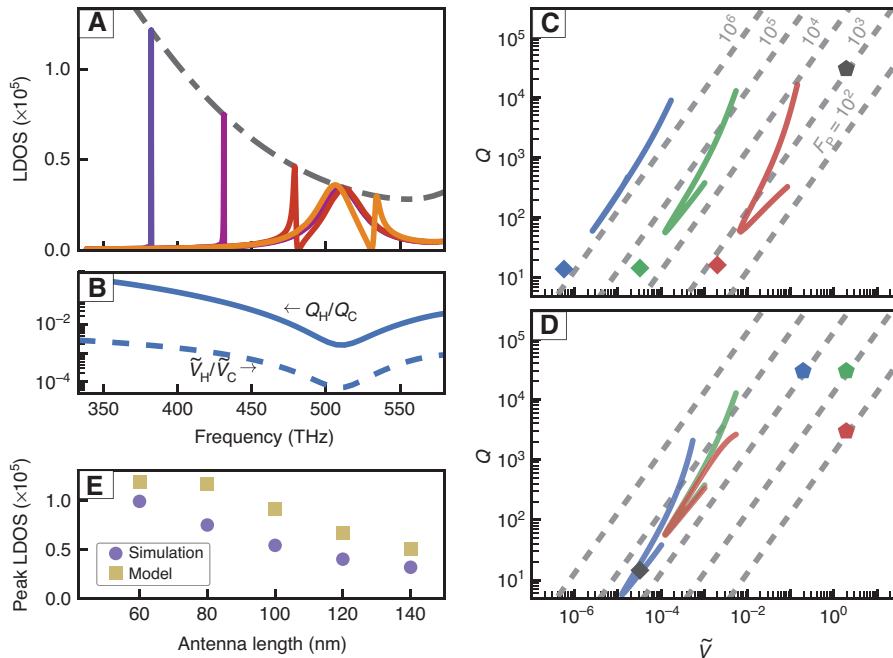


**Figure 4:** Hybrid design rules.

(A) LDOS spectra for four hybrids with different cavity resonance frequencies  $\omega_{\text{c}}$ . We fix  $Q_{\text{c}}$  and  $\tilde{V}_{\text{c}}$  to those of our nanobeam cavity, and let  $\omega_{\text{c}}$  change. The antenna is a gold dimer with ellipsoid length  $L = 80$  nm and a gap of 5 nm. The dash-dotted gray line indicates the envelope function describing hybrid peak LDOS as a function of  $\omega_{\text{c}}$ , and is given by  $3/(4\pi^2)Q_{\text{H}}/\tilde{V}_{\text{H}}$ , with  $Q_{\text{H}}$  and  $\tilde{V}_{\text{H}}$  given in Eqs. (4) and (5), respectively. (B) Hybrid quality factor  $Q_{\text{H}}$  and mode volume  $\tilde{V}_{\text{H}}$  relative to cavity values, as a function of  $\omega_{\text{c}}$ . We see a dramatic decrease of both  $Q_{\text{H}}$  and  $\tilde{V}_{\text{H}}$  near antenna resonance. (C) The effect of changing detuning and antenna mode volume on  $Q_{\text{H}}$  and  $\tilde{V}_{\text{H}}$ . Combining a nanobeam cavity (black marker) with antennas of  $L = 80$  nm and gaps of 1 (blue marker), 5 (green marker) and 25 nm (red marker), while letting  $\omega_{\text{c}}$  vary over the spectral range shown in (A, B), leads to hybrids with  $Q_{\text{H}}$  and  $\tilde{V}_{\text{H}}$  shown by the full curves (color corresponding to the antenna used). We see that  $Q_{\text{H}}$  and  $\tilde{V}_{\text{H}}$  are tunable through cavity-antenna detuning, and that  $\tilde{V}_{\text{H}}$  scales with antenna  $\tilde{V}$ . The dashed lines in (C) and (D) indicate constant  $F_{\text{p}}$ . (D) The effect of cavity  $Q$  and  $\tilde{V}$ . Similar to (C), we combine an antenna with  $L = 80$  nm and a gap of 5 nm (black marker) with either one of three nanobeam cavities, with  $Q_{\text{c}}$  and  $\tilde{V}_{\text{c}}$  as simulated (green marker), with a 10-fold reduced  $Q_{\text{c}}$  (red marker) or a 10-fold reduced  $\tilde{V}_{\text{c}}$  (blue marker). Hybrid parameters are indicated by the curves in the corresponding color. We see that a reduced  $\tilde{V}_{\text{c}}$  leads to an equal reduction in  $Q_{\text{H}}$  and  $\tilde{V}_{\text{H}}$ , and that  $Q_{\text{c}}$  only matters when  $Q_{\text{H}}$  approaches it. (E) Comparison between peak LDOS in hybrid systems of varying antenna length as obtained by finite element simulations of the full hybrid system (purple) and by the coupled oscillator model (yellow). Despite deviations, the model predicts the correct trend and order of magnitude.

of magnitude. The basic effect at work is captured by cavity perturbation theory, which states that the complex resonance frequency of a cavity will shift by  $\Delta\omega = -\omega\alpha/(\varepsilon_0\varepsilon V_c)$ . This implies a strong perturbation of  $Q_c$  only near antenna resonance (large imaginary  $\alpha$ ). Remarkably, the hybrid mode volume  $\tilde{V}_H$  experiences a similar trend as  $Q_H$ , thus keeping peak LDOS (i.e.  $Q_H/\tilde{V}_H$ ) roughly constant. This is shown by the envelope function in Figure 4A, which describes peak LDOS for varying detuning. While  $Q$  and  $V$  vary by orders of magnitude, LDOS varies only by a factor  $\sim 4$ . Letting cavity frequency  $\omega_c$  vary over the spectrum in Figure 4A while keeping the antenna constant results in  $Q-\tilde{V}$  curves, as shown in Figure 4C. Just by changing detuning, the hybrid  $Q$  and  $\tilde{V}$  can be changed over orders of magnitude at roughly constant LDOS.

- **Rule of thumb II:** better antennas make better hybrids. Figure 4C also displays the influence of the antenna mode volume. Decreasing the dimer gap size leads to significantly “better” antennas, meaning higher LDOS in the gap, or equivalently lower antenna mode volume. Figure 4C shows antennas and hybrids with gaps of 1, 5, and 25 nm. As antenna mode volume (i.e. gap size) is decreased, hybrid mode volumes decrease proportionally. This reflects the fact that hybrids enjoy the benefits of strong local antenna hotspots in the same manner as a bare antenna does. In other words, the emitter-antenna coupling (captured here in  $G_{bg}$ ) is not affected by the photonic environment of the antenna (i.e. the presence of a cavity). Indeed, from Eq. (3), we see that an increase of  $G_{bg}$  leads to an increase of  $LDOS_H$  as well.
- **Rule of thumb III:** decreasing cavity mode volume decreases both hybrid  $Q$  and  $\tilde{V}$ , while keeping LDOS fixed. Indeed, Figure 4D shows that a 10-fold decrease in cavity mode volume  $\tilde{V}_c$  simply shifts the hybrid parameters along the diagonal lines of constant LDOS. This is best understood by considering the expressions for  $Q_H$  and  $\tilde{V}_H$ , given as follows [29]:

$$Q_H = \omega_c \left( \kappa_c + \frac{\omega_c}{\varepsilon_0\varepsilon V_c} \text{Im}\{\alpha\} \right)^{-1}, \quad (4)$$

$$\tilde{V}_H = \frac{\tilde{V}_c}{|1 + \alpha G_{bg}|^2}, \quad (5)$$

where  $\kappa_c = \omega_c/Q_c$  is the bare cavity loss rate,  $\varepsilon_0$  is the vacuum permittivity, and  $\varepsilon$  is the relative permittivity of the antenna host medium. As long as the hybrid  $Q_H$  is dominated by antenna losses [i.e. the second term in Eq. (4)], both  $Q_H$  and  $\tilde{V}_H$  are proportional to the cavity mode volume  $\tilde{V}_c$ . Thus, decreasing  $\tilde{V}_c$  decreases

$Q_H$  and  $\tilde{V}_H$  equally, keeping LDOS constant. This behavior breaks down when cavity losses become dominant, which happens for large detuning (small  $\text{Im}\{\alpha\}$ ), and of course in bad cavities (low  $Q_c$  or large  $\tilde{V}_c$  to start with).

- **Rule of thumb IV:** bare cavity  $Q$  is irrelevant, unless the hybrid  $Q$  approaches it. As shown in Figure 4D, changing cavity quality factor has little influence on hybrid properties. Only when hybrid  $Q$  approaches that of the bare cavity, it is possible to gain any performance in Purcell factor by increasing the bare cavity  $Q$ . This is again well understood from Eqs. (4) and (5), which show that cavity losses do not affect  $\tilde{V}_H$ , and affect  $Q_H$  only when antenna losses are so small that cavity losses are dominant.

The strength of the coupled oscillator model used here to find these rules lies in its simplicity, even if they are not quantitatively accurate rules of thumb (only passably accurate on a log-log scale). For example, Figure 4E shows a comparison between peak LDOS in hybrid systems obtained directly from simulations of hybrids, and predicted by the model. We observe that the model correctly predicts the order of magnitude and the trend in peak LDOS as the antenna length is varied, although exact values deviate by up to a factor 2. This deviation is in fact easily solvable even within the analytical model. It is mainly caused by the fact that we retrieved antenna parameters in *complete absence* of the  $\text{Si}_3\text{N}_4$ , whereas in fact the nitride substrate induces an antenna redshift that is completely unrelated to the cavity resonance *per se*. Including this nonresonant shift largely resolves the discrepancy [29]. The rules of thumb discussed above can be used to understand the requirements for the components of a hybrid for different applications, which we will discuss in the following section.

## 4 Applications

The promise of hybrid plasmonic-photonic resonators is to provide resonances with linewidths intermediate between the constituent antenna and resonator, and mode volumes that cannot be reached by microcavities alone. We have now established by full-wave simulation that in principle a family of nanobeam-dimer antenna hybrids indeed allows deep subwavelength confinement, high  $Q$ , and high Purcell factor, and furthermore proposed four rules for the design of resonators with quality factors and mode volumes anywhere between those of the bare cavities and antennas. Exactly which combination of hybrid quality factor and mode volume is desirable depends on

the exact application one targets. In the following section, we focus on select applications in quantum optics, and discuss how hybrid systems can benefit these.

#### 4.1 Single-emitter single-photon strong coupling

Strong coupling between an optical (cavity) mode and a single emitter has long been pursued in the field of quantum optics. It is a cornerstone of cavity QED, as recognized by the 2012 Nobel prize for its realization in atomic physics [62], and is hotly pursued for on-chip quantum information processing with photons and matter in the benchmark material system of III-V semiconductors and quantum dots at liquid helium temperatures [13, 20, 21, 23]. A major promise of plasmonic antennas has been to provide room-temperature strong coupling of single emitters and light, using the exceptionally tight confinement and concomitantly large single-photon field strength to overcome the poor linewidth of emitters at room temperature. This regime has been claimed to be reached in select plasmonic nanogap antennas [17, 18, 50] that feature single-digit or sub-nanometer gaps.

In strong coupling, the emitter-cavity coupling is sufficiently strong for energy to be coherently exchanged between the emitter and the cavity before either the photon or the coherence of the emitter is lost. Experimentally, the signature is typically observed either by a spectral splitting in the frequency domain (vacuum Rabi splitting for a single emitter in a cavity), or by Rabi oscillations in the time domain. Strong coupling offers a route to create effective interactions between single photons, as the reflection of the cavity becomes different for, for example, single- and two-photon states due to the saturable absorption of the emitter, and the nonlinearity of the Jaynes-Cummings ladder [12].

The onset of the strong coupling regime occurs where the coupling rate between an emitter and a cavity system exceeds the sum of the loss rates [55, 63]:

$$2g > \kappa + \gamma_e, \quad (6)$$

where  $\kappa = \omega/Q$  is the loss rate of the cavity, and  $\gamma_e$  is the full linewidth of the emitter (including dephasing). The coupling rate  $g$  between the emitter and the cavity is given by

$$4g^2 = \kappa\gamma_e F_p = \gamma_e \frac{3}{4\pi^2} \frac{\omega}{\tilde{V}}, \quad (7)$$

where  $\omega$  is the frequency of the emitter transition and  $\gamma_e$  is its radiative decay rate. This decay rate differs from

the total decay rate  $\gamma_{\text{tot}}$ , which is the quantity usually obtained in lifetime measurements, by a factor which is the quantum efficiency QE, that is,  $\gamma_e = \gamma_{\text{tot}} \cdot \text{QE}$ . The radiative lifetime and emission frequency are related to the emitter's oscillator  $f$  strength via [55, 64]

$$f = \frac{2\mu^2 m_e \omega}{\hbar e^2}, \quad (8)$$

where  $m_e$  and  $e$  are the electron mass and charge, respectively, and

$$\mu = \sqrt{\gamma_e \frac{3\pi\epsilon_0 \hbar c^3}{n\omega^3}} \quad (9)$$

is the emitter's transition dipole moment. Here,  $n$  is the refractive index of the medium embedding the emitter. Using these equations, we can determine conditions that a resonator needs to satisfy for strong coupling if the emitter's emission frequency, linewidth, and radiative lifetime or oscillator strength are known.

##### 4.1.1 At room temperature

A starting point for the discussion is that any given emitter determines a characteristic curve in the  $Q-\tilde{V}$  diagram above which strong coupling is achieved. The condition for strong coupling in Eq. (6) yields a required minimum  $Q$  for an optical cavity at a given  $\tilde{V}$  for given emitter properties set by

$$Q > \frac{\omega}{\sqrt{\frac{3\omega\gamma_e}{4\pi^2\tilde{V}} - \gamma_e}}. \quad (10)$$

This condition is plotted for several emitters at room temperature in Figure 5A, which poignantly visualizes the different roles of the linewidth and the radiative lifetime of the emitter. The curves are typified by an inflection point at a critical combination of mode volume and  $Q$ . The emitter's radiative lifetime determines the left-right position of the curve: a faster radiative decay is equivalent to a larger oscillator strength, which shifts the curve to higher mode volumes, relaxing the strong coupling condition. At mode volumes  $\tilde{V}$  below the inflection point, the dominant inhibiting factor for strong coupling is if light is lost before a Rabi oscillation is completed. In this limit strong coupling can be achieved by increasing the quality factor of the cavity. If one traces the curve to higher  $\tilde{V}$ , increasing the  $Q$  to match, at some point the emitter dephasing rate becomes the limiting factor. From this point onward, no

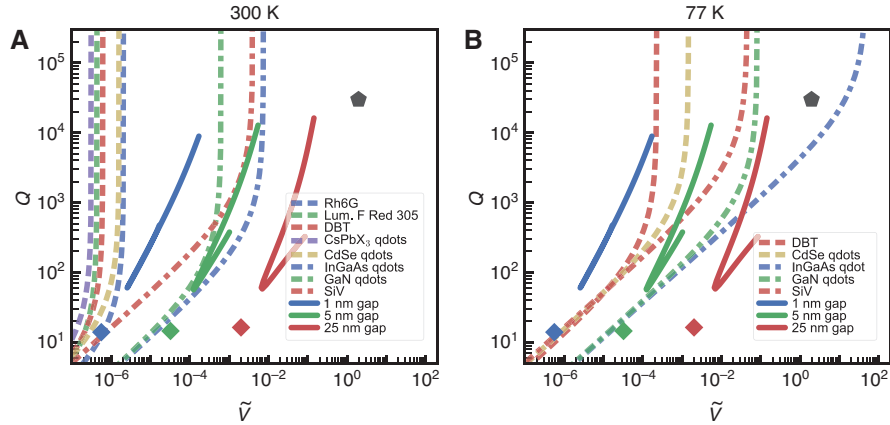


**Figure 5:** Strong coupling conditions for different emitters at room and liquid nitrogen temperatures.

We find a threshold for the mode volume above which strong coupling becomes impossible. Upon cooling the emitters to liquid nitrogen temperatures, this threshold is relaxed by several orders of magnitude. We show the same cavity (black marker), antennas (colored diamonds) and hybrids (full colored lines) as in Figure 4C. At room temperature,  $Q$ ,  $\tilde{V}$  are insufficient for strong coupling with most emitters. At 77 K, the reduced dephasing of the emitters relaxes the strong coupling condition such that the hybrids can reach strong coupling where the components cannot.

matter how much the  $Q$  is improved, the system cannot be brought to strong coupling. The only way out would be to reduce the mode volume, or alternatively to cool the emitter in order to reduce dephasing.

We have made an inventory of promising efficient single-photon emitters in the literature, taken from a pool of outstanding organic quantum emitters [17, 65–69], II-VI and III-V/III-N semiconductor quantum dots [70–77] and color centers [78]. The relevant properties of the emitters shown here are given in Table 1. For almost all single-photon emitters at room temperature, the linewidths are of order 20 to 50 THz. As such, we see that at room temperature, the minimum required mode volumes are invariably between  $10^{-5}$  and  $10^{-7}(\lambda/n)^3$ , irrespective of the  $Q$  that could be achieved. For reference, those systems for which room temperature strong coupling has been claimed have

$Q \sim 20$ , and claimed mode volumes from  $\sim 10^{-7}$  to  $10^{-6}(\lambda/n)^3$ , just sufficient for strong coupling. The exceptional emitters in this diagram are the SiV defect center in diamond and GaN and InGaAs quantum dots, which retain narrow zero-phonon lines at room temperature [75–78]. Unfortunately, these exceptions are also all but impossible to embed in a gap of a few nm, making them quite unusable for room-temperature strong coupling in a hybrid structure.

To assess if hybrid resonators will facilitate strong coupling, Figure 5 shows the  $Q$  and  $\tilde{V}$  values for the separate components and the curves for hybrid performance, for the three hybrids from Figure 4C. With the exception of SiV and InGaAs quantum dots, the hybrid curves do not reach the SC regime. At the smallest antenna gap size of 1 nm, the antenna could reach SC with a room-temperature

**Table 1:** Selection of emitters at room and liquid nitrogen temperatures.

Emitter	$\omega/2\pi$ (THz)	$\gamma_e/2\pi$ 300 K (THz)	$\gamma_e/2\pi$ 77 K (GHz)	$\gamma_{\text{tot}}/2\pi$ (MHz)	$n$	QY	$f$
DBT [65, 66]	380	38	2	208	1.59	0.24	5.5
Rh6G [67, 68]	535	47		172	1.5	0.98	10
Methylene blue [17, 69]	490	20		7.7	1.4	0.03	0.02
Lum. F Red 305 [67, 68]	490	81		126	1.5	0.91	8.1
CsPbX3 qdots [70]	545	64		67	1.5	0.7	2.7
CdSe/ZnSe qdots [71–74]	500	26	1000	61	1.5	0.8	3.3
GaN qdots [75, 76]	1050	10.9	970	3330	3.4	0.98	22
InGaAs qdots [77]	307	0.96	12	1000	3.4	1	79
SiV [78]	405	0.4	120	1000	2.4	0.05	3.2

Because in our calculations the emitter is assumed to be in vacuum, here we correct for the index of the surrounding medium (and for the quantum yield) when calculating oscillator strength of the emitter in vacuum, such that  $\gamma_0 = \gamma_{\text{tot}} \cdot \text{QE}/n$ .

dibenzoterrylene (DBT) molecule by itself, but the hybrid will not. This illustrates the difficulty of strong coupling with hybrids at room temperature. Compared to the bare antenna, hybrids gain in  $Q$  but unfortunately also in  $\tilde{V}$ . This means that hybrids are advantageous for high Purcell factors at any  $Q$ . At the same time, the peculiar upswing of the strong coupling curves at a critical mode volume means that hybrids are not advantageous for strong coupling at room temperature compared to the bare antenna. Antennas that will allow a hybrid system to reach strong coupling with a single emitter at room temperature will usually be able to reach it without the help of the cavity. Thus, while there could still be a benefit to have linewidth control, hybrids do not provide any alleviation of the nanofabrication problem involved in reaching room-temperature strong coupling. Similar conclusions can be gleaned from the work of Gurlek et al. [41]. They show that strong coupling could be possible in a tuneable-mirror cavity hybridized with a nanocone antenna, but only by virtue of the huge LDOS boost that the nanocone by itself provides.

#### 4.1.2 At 77 K

When temperature is reduced from room temperature, emitters become significantly more well behaved. Linewidths narrow as dephasing is reduced, while radiative lifetimes remain mostly unchanged [76–80]. A main technological advantage would be if at least liquid helium temperatures could be avoided for a platform based on single-emitter strong coupling, ideally reaching out to temperatures achievable with Peltier coolers ( $-100^\circ\text{C}$ ), or at least no colder than liquid nitrogen. Figure 5 shows that the condition on the mode volume is relaxed significantly at these temperatures. Here, the hybrid systems show a distinct improvement on the separate components, with strong coupling achievable for a variety of emitters, even in cases where the individual constituent cavity and antennas alone do not suffice. Moreover, it is possible for hybrid systems with gaps as large as 5 nm to reach strong coupling with nearly all emitters shown here, significantly outperforming its components. Hence, hybrids offer a practical route to strong coupling at 77 K – compared to cavities, they offer a larger choice in emitters and alleviate the demands on spectral alignment by operating at lower  $Q$ . Compared to antennas, spatial alignment criteria are relaxed since larger gap sizes (mode volumes) can be used. For this, one pays the price of a more complex, multi-step fabrication procedure.

## 4.2 Multiple-emitter strong coupling

Though the strong coupling of single-quantum emitters to a cavity mode is generally seen as the main path toward quantum optics on the basis of single-photon nonlinearities, currently many efforts are also put into achieving strong coupling with many emitters [81–86]. Strong coupling with multiple emitters is easier to achieve owing to the fact that the oscillator strength of an ensemble of  $N$  emitters effectively scales with  $\sqrt{N}$ , which facilitates strong coupling at larger mode volumes and lower quality factors. Figure 6 shows the strong coupling condition for 1,  $10^2$ , and  $10^4$  emitters. These emitters have a 100-MHz radiative decay rate  $\gamma_0$  (typical for organic molecules) and emit at 400 THz with a 1 THz linewidth, which lies between that of room temperature and liquid nitrogen temperature DBT molecules (see Table 1). The figure illustrates the benefit of an increased oscillator strength, where every factor of 100 emitters shifts the inflection point of the curves by an order of magnitude.

Strong coupling with ensembles of molecules is emerging as a topic of interest in several different fields. A main reason comes from the field of cavity exciton-polariton physics, where it is realized that intrinsically noninteracting photons become strongly interacting particles when hybridized with excitons into exciton polaritons [87, 88]. This is achieved in the multi-emitter strong

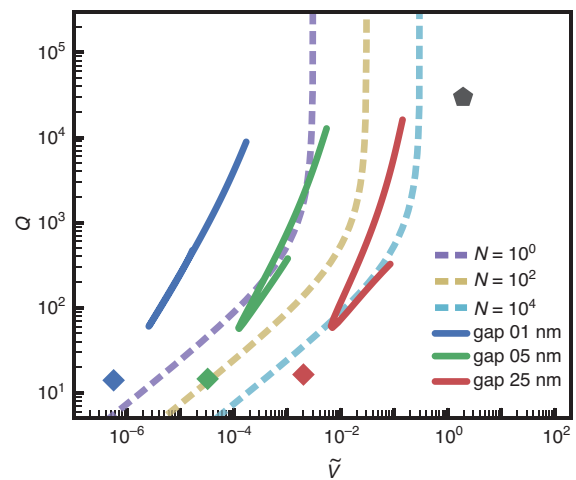


**Figure 6:** Strong coupling conditions for ensembles of emitters, at different emitter numbers  $N$ .

We use emitters with  $\gamma_0/2\pi = 100$  MHz,  $\gamma_e = 2\pi = 1$  THz and  $\omega/2\pi = 400$  THz. The oscillator strength scales with  $\sqrt{N}$ , and a factor of 100 in  $N$  shifts the condition for strong coupling by an order of magnitude in  $\tilde{V}$ . Note that even a  $20 \times 20 \times 1$  nm<sup>3</sup> gap could in principle fit over  $10^2$  molecular emitters. We show the same cavity (black marker), antennas (colored diamonds) and hybrids (full colored lines) as in Figures 4C and 5 for comparison.

coupling case. The resulting interacting quasiparticles are interesting as a realization of quantum superfluids that show phase transitions like condensation [89], superfluidity [90, 91], long-range coherence [92, 93] and nonlinear states [94]. Coupled arrays of cavity exciton-polariton systems could form the basis of quantum simulators [95, 96], a topic that is being pursued in organic and semiconductor exciton systems, as well as novel materials like perovskites [97, 98] and 2D transition metal dichalcogenides [99, 100]. From an optical point of view, these systems could mean a new venue in which to study quantum light sources, such as polariton lasers, and super- and subradiance phenomena. From a more matter-oriented point of view, Hutchison et al. [101, 102] pioneered the notion that the coupling of collective molecular resonances to an optical mode can alter chemical reaction energy landscapes, work functions, phase transitions, and electronic transport. Experiments show that ensembles of molecules coupled to optical cavities allow for optical and reversible switching between the weak- and ultrastrong coupling regime, with Rabi splittings that approach the molecular transition energy, and with tangible effects on chemical rate constants [81, 88, 101–105]. This line of research also extends to vibrational spectroscopy, in an emerging field coined (cavity-enhanced) molecular optomechanics. For example, scenarios of collective strong coupling of molecular vibrations to an (infrared) cavity resonance have been experimentally and theoretically considered in [84, 103], arguing that a macroscopic coherent superposition of molecular vibrations arises that behaves as a single mechanical oscillator. In a related context, researchers pursue Raman phenomena in plasmonic picocavities at the limit of strong coupling [50, 106]. An excellent review has appeared in this journal [107].

Hybrid plasmonic photonic resonators could provide a new venue for few/multi-emitter strong coupling. Currently, these types of room-temperature strong coupling experiments have used extended plasmonic lattices in order to obtain higher  $Q$  (order  $10^2$  higher than plasmonics alone provide), requiring molecules of the order of  $10^7$  per plasmon antenna [83]. In microcavity systems that displayed strong coupling with organic fluorophores [108], the number of dye molecules per cubic wavelength of device volume was similar within one order of magnitude. For room-temperature organic fluorophores, hybrids have no advantage over pure antenna systems, as discussed in Section 4.1.1. However, at slightly lower temperatures between liquid nitrogen and room temperature, perhaps even around those provided by Peltier coolers, hybrids do offer new opportunities. Figure 6 shows that hybrid plasmonic-photonic resonators could facilitate strong coupling

of few-emitter ensembles of organic molecules as small as 5 to 10, and upward, at quality factors that are 100 to a few thousand. This would thus allow to very controllably study cooperative phenomena in few-emitter systems. As the dominant loss channel of hybrids can be through the cavity input-output channels, one could really envision making individual “nodes” that are waveguide addressable, and that could be made to interact through integrated optics networks, in vein of quantum simulator demands. This should be contrasted to the extended microcavity and plasmon array systems studied in the literature. Also, one could envision creating interacting strongly coupled nodes by hybridizing a single cavity with *multiple* antennas, each coupled to a patch of molecular matter.

### 4.3 Single-photon sources: time jitter, brightness, and indistinguishability

Single-photon sources, essential for photonics quantum networks [3, 109], should fulfill a number of conditions: applications such as quantum key distribution require high repetition rates and low timing jitter, meaning that there should be low uncertainty in when the photon is emitted [110]. This is achieved by having a short lifetime, that is, placing the emitter in a high Purcell factor resonator. It also requires that the cavity and emitter should not be in the strong coupling regime, as this would increase jitter due to Rabi oscillations. Clearly, hybrids are excellent candidates for single-photon sources due to their high achievable Purcell factors that exceed those of the individual components. Moreover, as we have seen in Section 3, through cavity-antenna detuning the linewidth can be chosen to match that of the emitter, while keeping roughly the same Purcell factor. This facilitates the coupling to emitters at noncryogenic temperatures.

Any quantum optical process requiring single-photon sources benefits from high source brightness, meaning that the source should produce as many (single) photons per second as possible [3, 15, 110]. This relates again to the lifetime, as the repetition rate of the source can never be higher than the inverse lifetime, but also to radiative efficiency. Hence, if resonators are used to decrease emitter lifetimes, these resonators should not be too lossy. Again, hybrid systems have an advantage over only-plasmon antennas, because changing the resonator linewidth also changes the distribution of energy over the cavity and the (lossy) antenna. Hence, nonradiative antenna losses can be mitigated by going to the red-detuned regime where a large fraction of the energy exits the system via radiative cavity losses. In fact, it was shown that hybrid systems can

show highly efficient power extraction into a single-mode waveguide, while keeping LDOS high [35, 111].

Applications that rely on the interference between two single photons to create an effective photon-photon interaction, such as several schemes for quantum computation and communication [112, 113] or boson sampling [114, 115], also require these photons to be indistinguishable [19, 116]. This implies first excellent control over the polarization and optical mode that the photon is emitted into, and secondly emission spectra that are (close to) Fourier-transform limited [3], that is, no strong dephasing. Assuming that photons are always emitted into the same optical mode with the same polarization, the photon indistinguishability  $I$  produced by an emitter with a Purcell-enhanced radiative rate of  $F_p\gamma_0$  and a total linewidth  $\gamma_e$  (in the absence of the cavity, including dephasing and radiation into the background medium) is given as follows [64]:

$$I \approx \frac{F_p\gamma_0}{F_p\gamma_0 + \gamma_e}. \quad (11)$$

This implies that in the presence of dephasing, a minimum Purcell factor is required to achieve a desired indistinguishability. Moreover, to fully benefit from the Purcell enhancement provided by a resonator, one has to be in the “good emitter limit” [117], note that one could also operate in the bad emitter limit, but this typically comes at the cost of source brightness, as not all photons are emitted into the (cavity) bandwidth of interest. This means that the total emitter linewidth in the presence of the cavity should not exceed the cavity linewidth, that is

$$\gamma_e + F_p\gamma_0 \leq \kappa. \quad (12)$$

This condition also ensures that the device operates in the weak-coupling regime. Together, Eqs. (11) and (12) define a region in the  $Q-\tilde{V}$  diagram, specific for each emitter, in which good indistinguishability can be achieved. Figure 7 shows these regions for a selection of emitters and a minimum indistinguishability of 50%, at room temperature and at 77 K. We notice that only a narrow region is available for each emitter. High- $Q$  cavities often fall outside this region, mainly because these do not satisfy Eq. (12). Antennas appear a more natural choice (at these temperatures), yet in practice there is often another constraint to consider. Most emitters support multiple emission lines or phonon sidebands, often close in frequency to the emission line of interest. To avoid also enhancing these lines (thus decreasing indistinguishability), one typically tries to match the resonator  $Q$  as closely as possible to the width of this emission line. This implies that often, only the top parts of the shaded regions in Figure 7 are useful. This shows that to make a good single-photon source at high temperatures, good control over the exact  $Q$  and  $\tilde{V}$  of the resonator is essential. This is, of course, exactly what hybrids provide.

#### 4.4 High-speed LEDs, lasers, and label-free particle sensors

For a large number of applications besides spontaneous emission control, key figures of merit directly depend on the Purcell factor  $F_p$ . An obvious example is the modulation speed of an LED. LEDs could play a role in optical circuits,

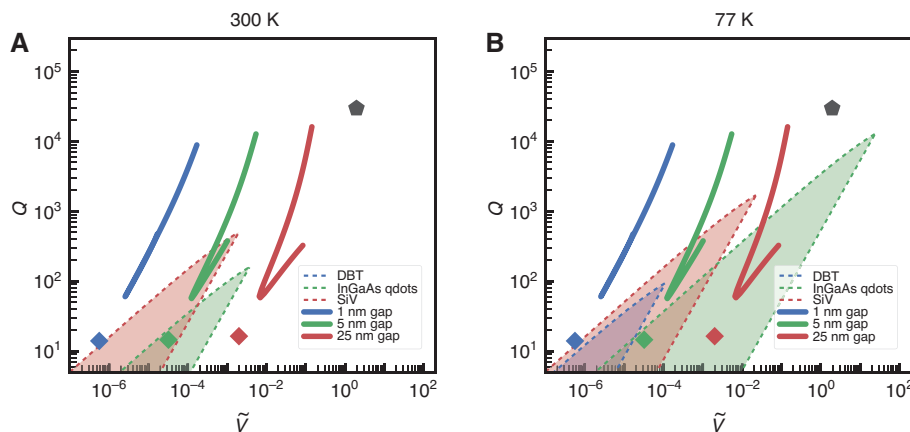


**Figure 7:** Conditions for indistinguishable photon sources, for different emitters at room temperature and 77 K.

Conditions on  $Q$  and  $\tilde{V}$  for indistinguishable photon emission at room temperature (A) and 77 K (B), for different emitters. We show  $Q$  and  $\tilde{V}$  of the same cavity, antennas and resulting hybrids as shown in Figures 4C and 5 (full curves and markers). Furthermore, for three emitters the shaded regions indicate the range of resonator  $Q$  and  $\tilde{V}$  for which a single-photon source with indistinguishability  $I \geq 50\%$  can be attained, i.e. Eqs. (11) and (12) are satisfied. Note that for DBT at 300 K, this region falls just outside the plot range. We show the same cavity (black marker), antennas (colored diamonds) and hybrids (full colored lines) as in Figures 4C, 5, and 6.

which have been proposed [118, 119] to replace electrical interconnects on a microprocessor. Owing to their many advantages compared to lasers, including energy-efficient operation, low cost, and high reliability, LEDs are attractive as light sources for such interconnects. However, LED switching speeds are currently limited to  $\sim 100$  MHz, approximately two orders of magnitude slower than a typical solid-state laser [119]. Since the switching rate of an LED is ultimately limited by the excited state lifetime of the carriers – although in practice also other limiting factors such as device capacitance may play a role – this rate scales proportionally with  $F_p$ . Moreover, enhancing the spontaneous emission rate additionally provides control over where the light is going [13], which enables, for example, directional emission or efficient collection of the light from such LEDs.

Purcell enhancements can also benefit the development of small, low-threshold lasers. Spontaneous emission and stimulated emission are intimately linked through the Einstein coefficients. It is therefore not surprising that, to first order, the pump power required to reach the lasing threshold is proportional to  $V/Q$ , with  $Q$  and  $V$  the quality factor and mode volume of the laser cavity mode [11]. Hence, large  $F_p$  decreases the minimal operation power of a laser, which can lead to a reduction of energy usage in optical communication [11, 119]. We note that in practice, the precise threshold power of a laser also depends on other (geometrical) parameters [120].

Besides influencing emission processes, the Purcell factor also plays a role in label-free optical particle detection. Optical resonators can be used to sense small particles such as single viruses or molecules [1, 10] through the fact that their resonance shifts when polarizable objects are placed in their near-field. Generic schemes to measure this shift convert the resonance shift in an intensity change for a narrow band laser tuned to the resonance edge in transmission or scattering. The detection sensitivity is determined by  $\Delta\omega/\kappa$ , that is, by the resonator lineshift  $\Delta\omega$  induced by the particle compared to the resonator linewidth. Cavity perturbation theory [61] states that, for a single small particle of polarizability  $\alpha_s$  perturbing a resonator,  $\Delta\omega \propto -\alpha_s/V$ . As a consequence, sensitivity is directly proportional to the Purcell factor.

LEDs, lasers, and particle sensors can clearly benefit from hybrid cavity-antenna systems, since these can achieve extremely large LDOS. In fact, hybrids have already been explored experimentally for nano-scale lasers and single-particle sensors. First hybrid lasers were demonstrated using a bow-tie antenna on a photonic crystal cavity [32, 33]; however, these did not harness the full potential of the device since the gain medium was embedded in the

photonic crystal, far from the antenna mode maximum. As particle sensors, hybrids have been experimentally studied extensively, particularly high- $Q$  whispering-gallery-mode cavities dressed by plasmonic antennas [25, 26, 28, 31, 37], with notable achievements including the detection of single ions in solution [121]. Note that, while hybrids are excellent as single-particle sensors, they prove less effective as bulk refractive index sensors [38].

## 4.5 Raman spectroscopy

Raman spectroscopy is based on the conversion of pump light to light at slightly up- or down-shifted frequency through an interaction with vibrations in a target material [122]. It is widely used to identify materials, as each material has its own unique spectroscopic vibrational fingerprint. Many efforts have been invested in increasing the poor efficiency of Raman processes, for example by harnessing the field confinement near a metallic surface or plasmonic antenna to boost pump intensity, and to boost the emission rate at the Stokes/anti-Stokes line [123–125]. To zeroth order, Raman signals are usually considered to scale as  $\eta_r \propto |E/E_0|^4$  (fourth power of “field enhancement”) [106, 122], yet Raman scattering is a two-frequency process, and efficiency factorizes as the product of pump field enhancement at frequency  $\omega_p$ , that is,  $|E(\omega_p)/E_0|^2$ , and the LDOS at the shifted frequency  $\omega_s$  [36]. While in plasmonics, resonances are so broad that pump-field enhancement and LDOS contributions are often near-identical, in microcavities, one can separately control the pump effect and Raman emission [39, 126, 127]. Hybrid cavity-antenna resonators could provide a unique venue here. Since the hot spot is pulled out of the cavity and into the antenna gap, it is directly available for the Raman-active species under investigation. At the same time, the hybridization of resonances, especially when considering the possibility of engaging several cavity modes and one antenna, could allow us to independently structure the enhancement factors at pump, Stokes and anti-Stokes frequency, judiciously matching resonances and their linewidths. This could be an especially exciting direction in the molecular optomechanics paradigm proposed by Roelli et al. [50, 106, 128].

## 5 Conclusion

In this work we have quantitatively assessed the merits of hybrid plasmonic-dielectric cavity-antenna systems,

focusing on the achievable trade-off in confinement and quality factor, and the merits for diverse applications. For this we have performed a systematic survey of performance metrics achievable in hybrids composed of a state-of-the-art high- $Q$  nanobeam cavity and a family of plasmon-gap antennas, where the gap size tunes the bare antenna LDOS. Full-wave simulations and a simple analytical model all confirm that a large freedom over  $Q$ , on par with those of microcavities, and  $\tilde{V}$ , deeply subwavelength, is possible within a set of four “rules of thumb.” These are that (1) antenna-cavity detuning controls hybrid  $Q$ , at hybrid  $Q/\tilde{V}$  that remains on par with the peak antenna LDOS, (2) better antennas in terms of LDOS make better hybrids, (3) more cavity confinement helps more confinement in the resulting hybrids, again at constant  $Q/\tilde{V}$ , and (4) the cavity  $Q$  is quite irrelevant unless one targets hybrids with similarly high  $Q$ . By themselves these “rules of thumb” are approximate, that is, accurate on our log-log plots. With parameters extracted from full-wave simulations for the individual components, the analytical model makes them quantitative for hybrids.

In excellent agreement with previous reports of several groups [27, 28, 30, 34, 35, 40, 41, 129], hybrids can outperform the individual constituents in terms of Purcell factor, and can do so at any  $Q$  that bridges the gap between the antenna and high- $Q$  cavity. Detuning allows one to choose  $Q$  while keeping  $F_p$  almost constant. The fact that this performance is available is a remarkable result in itself, as the mechanism by which hybrids operate is through delicate interferences, and not through, for example, an incoherent addition or multiplication of metrics. These interferences are directly visible in calculated LDOS lineshapes (Figure 4A) that show an entire family of Fano lines going from LDOS enhancement to transparency. Notably, achieving a narrow LDOS peak at plasmonic LDOS values is best *not* achieved by choosing plasmon-antenna and cavity *both* on resonance with the emitter.

The main purpose of this paper was to critically assess not only the accessible performance metrics, but also if they are of use for challenges set by promises of, for instance, the plasmonic quantum optics community. The fact that phenomenally high Purcell factors at a tunable quality factor are available is a big advantage for those applications that require a high Purcell factor, yet not strong coupling. These are for instance the development of room-temperature ultra-bright sources of single photons on demand, where  $Q$ -control is a crucial parameter for photon indistinguishability. Moreover, the

fact that hybrids can be designed to have all their loss through cavity loss channels, such as critically coupled waveguides, helps photon collection efficiency exceed the values achieved in ultra-high Purcell factor nanoantennas so far [14, 15].

Intuitively, one might think that the fact that *very* high Purcell factors are in reach also widens the prospects for room-temperature quantum strong coupling with single emitters, a feat so far claimed only to occur in select plasmon antennas with single-digit nanometric gaps [17, 18]. However, for this scenario, the huge dephasing rates reported in the literature for actual emitters at room temperature mean that extremely small mode volumes are necessary for strong coupling to a single emitter, regardless of  $Q$ . As a consequence, hybrid cavity-antenna structures that excel at  $Q$ , but only at moderately subwavelength confinement, cannot provide strong coupling conditions for any emitter at room temperature except maybe the SiV color center in diamond. Moreover, the geometrical requirements in terms of the ultra-narrow gaps that are required for strong coupling are in no way alleviated by the hybrid structure. These findings rationalize reports by Dezfouli et al. [43] and Gurlek et al. [41] that pointed out hybrids as highly promising for strong coupling, but for that needed exotic antenna shapes or gaps.

A useful niche could be in reaching strong coupling at liquid nitrogen temperatures, a regime that is significantly less demanding for real-life applications than the current liquid helium conditions of solid-state quantum optics. In this temperature regime dephasing decreases and higher mode volumes are allowed. Consequently, strong coupling is possible with a host of different emitter choices in hybrids at relaxed fabrication conditions, where neither the antenna nor the cavity alone would suffice, and where hybrids offer a large flexibility in choosing  $Q$ . Thus, hybrids can offer strong coupling at both relaxed spectral alignment criteria (lower  $Q$ ), as compared to the cavity, and relaxed spatial alignment and fabrication criteria (smaller gaps) as compared to the antenna. Finally, hybrids can also have applications outside single-emitter optics. These include few/many-emitter strong coupling in vein of work on the interface of chemistry and polaritonics, high-speed LEDs, low-threshold nano-scale lasers and single-particle sensing.

**Acknowledgments:** This work is part of the research program of the Netherlands Organization for Scientific Research (NWO). AFK acknowledges an NWO Vici grant, Funder Id: <http://dx.doi.org/10.13039/501100003246>.

## References

- [1] Vollmer F, Yang L. Label-free detection with high-Q microcavities: a review of biosensing mechanisms for integrated devices. *Nanophotonics* 2012;1:267–91.
- [2] Aspelmeyer M, Kippenberg TJ, Marquardt F. Cavity optomechanics. *Rev Mod Phys* 2014;86:1391–452.
- [3] Lounis B, Orrit M. Single-photon sources. *Rep Prog Phys* 2005;68:1129–79.
- [4] Aharonovich I, Englund D, Toth M. Solid-state single-photon emitters. *Nat Photonics* 2016;10:631–41.
- [5] Senellart P, Solomon G, White A. High-performance semiconductor quantum-dot single-photon sources. *Nat Nanotechnol* 2017;12:1026–39.
- [6] Raimond JM, Brune M, Haroche S. Manipulating quantum entanglement with atoms and photons in a cavity. *Rev Mod Phys* 2001;73:565–82.
- [7] Purcell EM. Spontaneous emission probabilities at radio frequencies. *Phys Rev* 1946;69:681.
- [8] Novotny L, Hecht B. Principles of nano-optics. 2nd ed. New York: Cambridge University Press, 2012.
- [9] Sprink R, van Tiggelen BA, Lagendijk A. Optical emission in periodic dielectrics. *Europhys Lett* 1996;35:265–70.
- [10] Vollmer F, Arnold S. Whispering-gallery-mode biosensing: label-free detection down to single molecules. *Nat Methods* 2008;5:591–6.
- [11] Hill MT, Gather MC. Advances in small lasers. *Nat Photonics* 2014;8:908–18.
- [12] Chang DE, Vuletić V, Lukin MD. Quantum nonlinear optics – photon by photon. *Nat Photonics* 2014;8:685–94.
- [13] Lodahl P, Mahmoodian S, Stobbe S. Interfacing single photons and single quantum dots with photonic nanostructures. *Rev Mod Phys* 2015;87:347–400.
- [14] Russell KJ, Liu TL, Cui S, Hu EL. Large spontaneous emission enhancement in plasmonic nanocavities. *Nat Photonics* 2012;6:459–62.
- [15] Akselrod GM, Argyropoulos C, Hoang TB, et al. Probing the mechanisms of large Purcell enhancement in plasmonic nanoantennas. *Nat Photonics* 2014;8:835–40.
- [16] Bidault S, Devilez A, Maillard V, et al. Picosecond lifetimes with high quantum yields from single-photon-emitting colloidal nanostructures at room temperature. *ACS Nano* 2016;10:4806–15.
- [17] Chikkaraddy R, de Nijs B, Benz F, et al. Single-molecule strong coupling at room temperature in plasmonic nanocavities. *Nature* 2016;535:127–30.
- [18] Groß H, Hamm JM, Tufarelli T, Hess O, Hecht B. Near-field strong coupling of single quantum dots. *Sci Adv* 2018;4:eaar4906.
- [19] Somaschi N, Giesz V, De Santis L, et al. Near-optimal single-photon sources in the solid state. *Nat Photonics* 2016;10:340–5.
- [20] Reithmaier JP, Sek G, Löffler A, et al. Strong coupling in a single quantum dot-semiconductor microcavity system. *Nature* 2004;432:197–200.
- [21] Yoshie T, Scherer A, Hendrickson J, et al. Vacuum Rabi splitting with a single quantum dot in a photonic crystal nanocavity. *Nature* 2004;432:200–3.
- [22] Reinhard A, Volz T, Winger M, et al. Strongly correlated photons on a chip. *Nat Photonics* 2012;6:93–6.
- [23] Peter E, Senellart P, Martrou D, et al. Exciton-photon strong-coupling regime for a single quantum dot embedded in a microcavity. *Phys Rev Lett* 2005;95:067401.
- [24] Srinivasan K, Painter O. Linear and nonlinear optical spectroscopy of a strongly coupled microdisk-quantum dot system. *Nature* 2007;450:862–5.
- [25] Shopova SI, Blackledge CW, Rosenberger AT. Enhanced evanescent coupling to whispering-gallery modes due to gold nanorods grown on the microresonator surface. *Appl Phys B* 2008;93:183–7.
- [26] De Angelis F, Patrini M, Das G, et al. A hybrid plasmonic-photonic nanodevice for label-free detection of a few molecules. *Nano Lett* 2008;8:2321–7.
- [27] Barth M, Schietinger S, Fischer S, et al. Nanoassembled plasmonic-photonic hybrid cavity for tailored light-matter coupling. *Nano Lett* 2010;10:891–5.
- [28] Santiago-Cordoba MA, Cetinkaya M, Boriskina SV, Vollmer F, Demirel MC. Ultrasensitive detection of a protein by optical trapping in a photonic-plasmonic microcavity. *J Biophotonics* 2012;5:629–38.
- [29] Frimmer M, Koenderink AF. Superemitters in hybrid photonic systems: a simple lumping rule for the local density of optical states and its breakdown at the unitary limit. *Phys Rev B* 2012;86:235428.
- [30] Xiao YF, Liu YC, Li BB, Chen YL, Li Y, Gong Q. Strongly enhanced light-matter interaction in a hybrid photonic-plasmonic resonator. *Phys Rev A* 2012;85:031805.
- [31] Dantham VR, Holler S, Barbre C, Keng D, Kolchenko V, Arnold S. Label-free detection of single protein using a nanoplasmonic-photonic hybrid microcavity. *Nano Lett* 2013;13:3347–51.
- [32] Zhang T, Belarouci A, Callard S, et al. Far-field and near-field investigation of plasmonic-photonic hybrid laser mode. *arXiv* 2014;1411.7201:1–12.
- [33] Zhang T, Callard S, Jamois C, Chevalier C, Feng D, Belarouci A. Plasmonic-photonic crystal coupled nanolaser. *Nanotechnology* 2014;25:315201.
- [34] Hong Y, Ahn W, Boriskina SV, Zhao X, Reinhard BM. Directed assembly of optoplasmonic hybrid materials with tunable photonic-plasmonic properties. *J Phys Chem Lett* 2015;6:2056–64.
- [35] Dooelman HM, Verhagen E, Koenderink AF. Antenna-cavity hybrids: matching polar opposites for Purcell enhancements at any linewidth. *ACS Photonics* 2016;3:1943–51.
- [36] Dezfouli MK, Gordon R, Hughes S. Modal theory of modified spontaneous emission of a quantum emitter in a hybrid plasmonic photonic-crystal cavity system. *Phys Rev A* 2017;95:013846.
- [37] Liang F, Guo Y, Hou S, Quan Q. Photonic-plasmonic hybrid single-molecule nanosensor measures the effect of fluorescent labels on DNA-protein dynamics. *Sci Adv* 2017;3:e1602991.
- [38] Bozzola A, Perotto S, De Angelis F. Hybrid plasmonic-photonic whispering gallery mode resonators for sensing: a critical review. *Analyst* 2017;142:883–98.
- [39] Liu JN, Huang Q, Liu KK, Singamaneni S, Cunningham BT. Nanoantenna-microcavity hybrids with highly cooperative plasmonic-photonic coupling. *Nano Lett* 2017;17:7569–77.
- [40] Thakkar N, Rea MT, Smith KC, et al. Sculpting Fano resonances to control photonic-plasmonic hybridization. *Nano Lett* 2017;17:6927–34.

- [41] Gurlek B, Sandoghdar V, Martín-Cano D. Manipulation of quenching in nanoantenna-emitter systems enabled by external detuned cavities: a path to enhance strong-coupling. *ACS Photonics* 2018;5:456–61.
- [42] Deotare PB, McCutcheon MW, Frank IW, Khan M, Lončar M. High quality factor photonic crystal nanobeam cavities. *Appl Phys Lett* 2009;94:121106.
- [43] Dezfouli MK, Gordon R, Hughes S. Molecular optomechanics in the anharmonic cavity-QED regime using hybrid metal-dielectric cavity modes. *ACS Photonics* 2019; DOI: 10.1021/acsp Photonics.8b01091.
- [44] Grande M, Calo G, Petruzzelli V, D’Orazio A. High-Q photonic crystal nanobeam cavity based on a silicon nitride membrane incorporating fabrication imperfections and a low-index material layer. *Prog Electromagn Res B* 2012;37:191–204.
- [45] Koenderink AF. On the use of Purcell factors for plasmon antennas. *Opt Lett* 2010;35:4208–10.
- [46] Sauvan C, Hugonin JP, Maksymov IS, Lalanne P. Theory of the spontaneous optical emission of nanosize photonic and plasmon resonators. *Phys Rev Lett* 2013;110:237401.
- [47] Ryckman JD, Weiss SM. Low mode volume slotted photonic crystal single nanobeam cavity in silicon. In: *The 9th International Conference on Group IV Photonics (GFP)*, Vol. 071104. IEEE, 2012, 24–6.
- [48] Seidler P, Lister K, Drechsler U, Hofrichter J, Stöferle T. Slotted photonic crystal nanobeam cavity with an ultrahigh quality factor-to-mode volume ratio. *Opt Express* 2013;21:32468.
- [49] Hu S, Khater M, Salas-Montiel R, et al. Experimental realization of deep-subwavelength confinement in dielectric optical resonators. *Sci Adv* 2018;4:eaat2355.
- [50] Benz F, Schmidt MK, Dreismann A, et al. Single-molecule optomechanics in “picocavities”. *Science* 2016;354:726–9.
- [51] Economou EN. Surface plasmons in thin films. *Phys Rev* 1969;182:539–54.
- [52] Bozhevolnyi SI, Søndergaard T. General properties of slow-plasmon resonant nanostructures: nano-antennas and resonators. *Opt Express* 2007;15:10869.
- [53] Yang J, Sauvan C, Jouanin A, Collin S, Pelouard JL, Lalanne P. Ultrasmall metal-insulator-metal nanoresonators: impact of slow-wave effects on the quality factor. *Opt Express* 2012;20:16880.
- [54] Faggiani R, Yang J, Lalanne P. Quenching, plasmonic, and radiative decays in nanogap emitting devices. *ACS Photonics* 2015;2:1739–44.
- [55] Marquier F, Sauvan C, Greffet JJ. Revisiting quantum optics with surface plasmons and plasmonic resonators. *ACS Photonics* 2017;4:2091–101.
- [56] Kristensen PT, Van Vlack C, Hughes S. Generalized effective mode volume for leaky optical cavities. *Opt Lett* 2012;37:1649–51.
- [57] Fano U. Effects of configuration interaction on intensities and phase shifts. *Phys Rev* 1961;124:1866–78.
- [58] Ruesink F, Doeleman HM, Hendriks R, Koenderink AF, Verhagen E. Perturbing open cavities: anomalous resonance frequency shifts in a hybrid cavity-nanoantenna system. *Phys Rev Lett* 2015;115:203904.
- [59] Bohren CF, Huffman DR. *Absorption and scattering of light by small particles*. New York: John Wiley & Sons, 1983.
- [60] Waldron RA. Perturbation theory of resonant cavities. *Proc IEE C* 1960;107:272.
- [61] Bethe H, Schwinger J. *Perturbation theory for cavities*. Cambridge, MA: Massachusetts Institute of Technology, Radiation Laboratory, 1943.
- [62] Haroche S. Nobel lecture: controlling photons in a box and exploring the quantum to classical boundary. *Rev Mod Phys* 2013;85:1083–102.
- [63] Auffèves A, Gerace D, Gérard JM, Santos MF, Andreani LC, Poizat JP. Controlling the dynamics of a coupled atom-cavity system by pure dephasing. *Phys Rev B* 2010;81:245419.
- [64] Santori C, Fattal D, Yamamoto Y. *Single-photon devices and applications*. Weinheim: John Wiley & Sons, 2010.
- [65] Toninelli C, Early K, Breimi J, Renn A, Göttinger S, Sandoghdar V. Near-infrared single-photons from aligned molecules in ultrathin crystalline films at room temperature. *Opt Express* 2010;18:6577.
- [66] Kwadrin A, Koenderink AF. Gray-tone lithography implementation of Drexhage’s method for calibrating radiative and nonradiative decay constants of fluorophores. *J Phys Chem C* 2012;116:16666–73.
- [67] Green AP, Buckley AR. Solid state concentration quenching of organic fluorophores in PMMA. *Phys Chem Chem Phys* 2015;17:1435–40.
- [68] Guo K, Lozano G, Verschuuren MA, Gómez Rivas J. Control of the external photoluminescent quantum yield of emitters coupled to nanoantenna phased arrays. *J Appl Phys* 2015;118:073103.
- [69] Olmsted J. Calorimetric determinations of absolute fluorescence quantum yields. *J Phys Chem* 1979;83:2581–4.
- [70] Protesescu L, Yakunin S, Bodnarchuk MI, et al. Nanocrystals of cesium lead halide perovskites (CsPbX<sub>3</sub>, X = Cl, Br, and I): novel optoelectronic materials showing bright emission with wide color gamut. *Nano Lett* 2015;15:3692–6.
- [71] Leistikow MD, Johansen J, Kettelarij AJ, Lodahl P, Vos WL. Size-dependent oscillator strength and quantum efficiency of CdSe quantum dots controlled via the local density of states. *Phys Rev B* 2009;79:045301.
- [72] Lunnemann P, Rabouw FT, van Dijk-Moes RJA, Pietra F, Vanmaekelbergh D, Koenderink AF. Calibrating and controlling the quantum efficiency distribution of inhomogeneously broadened quantum rods by using a mirror ball. *ACS Nano* 2013;7:5984–92.
- [73] Odoi MY, Hammer NI, Early KT, et al. Fluorescence lifetimes and correlated photon statistics from single CdSe/Oligo(phenylene vinylene) composite nanostructures. *Nano Lett* 2007;7:2769–73.
- [74] Sebald K, Michler P, Passow T, Hommel D, Bacher G, Forchel A. Single-photon emission of CdSe quantum dots at temperatures up to 200 K. *Appl Phys Lett* 2002;81:2920–2.
- [75] Choi K, Kako S, Holmes MJ, Arita M, Arakawa Y. Strong exciton confinement in site-controlled GaN quantum dots embedded in nanowires. *Appl Phys Lett* 2013;103:171907.
- [76] Yang W, Li J, Zhang Y, et al. High density GaN/AlN quantum dots for deep UV LED with high quantum efficiency and temperature stability. *Sci Rep* 2015;4:5166.
- [77] Bayer M, Forchel A. Temperature dependence of the exciton homogeneous linewidth in InGaAs/GaAs self-assembled quantum dots. *Phys Rev B* 2002;65:041308.
- [78] Neu E, Hepp C, Hauschild M, et al. Low-temperature investigations of single silicon vacancy colour centres in diamond. *New J Phys* 2013;15:043005.

- [79] Zhelezko FB, Gulis IM, Lounis B, Orrit M. Spectroscopic characteristics of single dibenzanthanthrene molecules isolated in a low-temperature naphthalene matrix. *J Appl Spectrosc* 1999;66:344–52.
- [80] Boiron AM, Lounis B, Orrit M. Single molecules of dibenzanthanthrene in n-hexadecane. *J Chem Phys* 1996;105:3969–74.
- [81] Ebbesen TW. Hybrid light-matter states in a molecular and material science perspective. *Acc Chem Res* 2016;49:2403–12.
- [82] Kasprzak J, Richard M, Kundermann S, et al. Bose–Einstein condensation of exciton polaritons. *Nature* 2006;443:409–14.
- [83] Ramezani M, Le-Van Q, Halpin A, Gómez Rivas J. Nonlinear emission of molecular ensembles strongly coupled to plasmonic lattices with structural imperfections. *Phys Rev Lett* 2018;121:243904.
- [84] Shalabney A, George J, Hutchison J, Pupillo G, Genet C, Ebbesen TW. Coherent coupling of molecular resonators with a microcavity mode. *Nat Commun* 2015;6:5981.
- [85] Li RQ, Hernández-Pérez D, García-Vidal FJ, Fernández-Domínguez AI. Transformation optics approach to plasmon-exciton strong coupling in nanocavities. *Phys Rev Lett* 2016;117:107401.
- [86] del Pino J, García-Vidal FJ, Feist J. Exploiting vibrational strong coupling to make an optical parametric oscillator out of a Raman laser. *Phys Rev Lett* 2016;117:277401.
- [87] Sanvitto D, Kéna-Cohen S. The road towards polaritonic devices. *Nat Mater* 2016;15:1061–73.
- [88] Törmä P, Barnes WL. Strong coupling between surface plasmon polaritons and emitters: a review. *Rep Prog Phys* 2015;78:013901.
- [89] Byrnes T, Kim NY, Yamamoto Y. Exciton–polariton condensates. *Nat Phys* 2014;10:803–13.
- [90] Lerario G, Fieramosca A, Barachati F, et al. Room-temperature superfluidity in a polariton condensate. *Nat Phys* 2017;13:837–41.
- [91] Amo A, Lefrère J, Pigeon S, et al. Superfluidity of polaritons in semiconductor microcavities. *Nat Phys* 2009;5:805–10.
- [92] Fischer J, Savenko IG, Fraser MD, et al. Spatial coherence properties of one dimensional exciton-polariton condensates. *Phys Rev Lett* 2014;113:203902.
- [93] Su R, Wang J, Zhao J, et al. Room temperature long-range coherent exciton polariton condensate flow in lead halide perovskites. *Sci Adv* 2018;4:eaau0244.
- [94] Gulevich DR, Yudin D, Skryabin DV, Iorsh IV, Shelykh IA. Exploring nonlinear topological states of matter with exciton-polaritons: edge solitons in kagome lattice. *Sci Rep* 2017;7:1780.
- [95] Feynman RP. Simulating physics with computers. *Int J Theor Phys* 1982;21:467–88.
- [96] Lloyd S. Universal quantum simulators. *Science* 1996;273:1073–8.
- [97] Du W, Zhang S, Zhang Q, Liu X. Recent progress of strong exciton-photon coupling in lead halide perovskites. *Adv Mater* 2018;1804894. <https://doi.org/10.1002/adma.201804894>.
- [98] Wang J, Su R, Xing J, et al. Room temperature coherently coupled exciton–polaritons in two-dimensional organic–inorganic perovskite. *ACS Nano* 2018;12:8382–9.
- [99] Kleemann ME, Chikkaraddy R, Alexeev EM, et al. Strong-coupling of WSe<sub>2</sub> in ultra-compact plasmonic nanocavities at room temperature. *Nat Commun* 2017;8:1296.
- [100] Munkhbat B, Baranov DG, Stührenberg M, Wersäll M, Bisht A, Shegai T. Self-hybridized exciton-polaritons in multilayers of transition metal dichalcogenides for efficient light absorption. *ACS Photonics* 2019;6:139–47.
- [101] Hutchison JA, Schwartz T, Genet C, Devaux E, Ebbesen TW. Modifying chemical landscapes by coupling to vacuum fields. *Angew Chem Int Ed* 2012;51:1592–6.
- [102] Hutchison JA, Liscio A, Schwartz T, et al. Tuning the work-function via strong coupling. *Adv Mater* 2013;25:2481–5.
- [103] del Pino J, Feist J, Garcia-Vidal FJ. Quantum theory of collective strong coupling of molecular vibrations with a microcavity mode. *New J Phys* 2015;17:053040.
- [104] Schwartz T, Hutchison JA, Genet C, Ebbesen TW. Reversible switching of ultrastrong light-molecule coupling. *Phys Rev Lett* 2011;106:196405.
- [105] Orgiu E, George J, Hutchison JA, et al. Conductivity in organic semiconductors hybridized with the vacuum field. *Nat Mater* 2015;14:1123–9.
- [106] Roelli P, Galland C, Piro N, Kippenberg TJ. Molecular cavity optomechanics as a theory of plasmon-enhanced Raman scattering. *Nat Nanotechnol* 2016;11:164–9.
- [107] Flick J, Rivera N, Narang P. Strong light-matter coupling in quantum chemistry and quantum photonics. *Nanophotonics* 2018;7:1479–501.
- [108] Lidzey D, Bradley D, Skolnick M, Virgili T, Walker S, Whittaker D. Strong exciton-photon coupling in an organic semiconductor microcavity. *Nature* 1998;395:53–5.
- [109] O’Brien JL, Furusawa A, Vučković J. Photonic quantum technologies. *Nat Photonics* 2009;3:687–95.
- [110] Gisin N, Ribordy G, Tittel W, Zbinden H. Quantum cryptography. *Rev Mod Phys* 2002;74:145–95.
- [111] Zhu G, Liao Q. Highly efficient collection for photon emission enhanced by the hybrid photonic-plasmonic cavity. *Opt Express* 2018;26:31391.
- [112] Knill E, Laflamme R, Milburn GJ. A scheme for efficient quantum computation with linear optics. *Nature* 2001;409:46–52.
- [113] Duan LM, Lukin MD, Cirac JJ, Zoller P. Long-distance quantum communication with atomic ensembles and linear optics. *Nature* 2001;414:413–8.
- [114] Broome MA, Fedrizzi A, Rahimi-Keshari S, et al. Photonic boson sampling in a tunable circuit. *Science* 2013;339:794–8.
- [115] Spagnolo N, Vitelli C, Bentivegna M, et al. Experimental validation of photonic boson sampling. *Nat Photonics* 2014;8:615–20.
- [116] Santori C, Fattal D, Vučković J, Solomon GS, Yamamoto Y. Indistinguishable photons from a single-photon device. *Nature* 2002;419:594–7.
- [117] Pitanti A, Ghulinyan M, Navarro-Urrios D, Pucker G, Pavesi L. Probing the spontaneous emission dynamics in Si-nanocrystals-based microdisk resonators. *Phys Rev Lett* 2010;104:103901.
- [118] Miller D. Device requirements for optical interconnects to silicon chips. *Proc IEEE* 2009;97:1166–85.
- [119] Tsakmakidis KL, Boyd RW, Yablonovitch E, Zhang X. Large spontaneous-emission enhancements in metallic nanostructures: towards LEDs faster than lasers. *Opt Express* 2016;24:17916.
- [120] Liu K, Sun S, Majumdar A, Sorger VJ. Fundamental scaling laws in nanophotonics. *Sci Rep* 2016;6:37419.
- [121] Baaske MD, Vollmer F. Optical observation of single atomic ions interacting with plasmonic nanorods in aqueous solution. *Nat Photonics* 2016;10:733–9.

- [122] Long DA. The Raman effect. Chichester, United Kingdom: John Wiley & Sons Ltd, 2002.
- [123] Kneipp K, Wang Y, Kneipp H, et al. Single molecule detection using surface-enhanced Raman scattering (SERS). *Phys Rev Lett* 1997;78:1667–70.
- [124] Nie S. Probing single molecules and single nanoparticles by surface-enhanced Raman scattering. *Science* 1997;275:1102–6.
- [125] Schatz GC, Young MA, Van Duyn RP. Electromagnetic mechanism of SERS. In: *Surface-enhanced Raman scattering*. Berlin/Heidelberg: Springer-Verlag, 2006, 19–45.
- [126] Huang SH, Jiang X, Peng B, et al. Surface-enhanced Raman scattering on dielectric microspheres with whispering gallery mode resonance. *Photonics Res* 2018;6:346.
- [127] Hümmer T, Noe J, Hofmann MS, Hänsch TW, Högele A, Hunger D. Cavity-enhanced Raman microscopy of individual carbon nanotubes. *Nat Commun* 2016;7:12155.
- [128] Schmidt MK, Esteban R, Benz F, Baumberg JJ, Aizpurua J. Linking classical and molecular optomechanics descriptions of SERS. *Faraday Discuss* 2017;205:31–65.
- [129] Boriskina SV, Reinhard BM. Spectrally and spatially configurable superlenses for optoplasmonic nanocircuits. *Proc Natl Acad Sci USA* 2011;108:3147–51.

---

**Supplementary Material:** The online version of this article offers supplementary material (<https://doi.org/10.1515/nanoph-2019-0062>).